ELSEVIER

Catalysis Today 77 (2003) 359–370

CATALYSIS TODAY

www.elsevier.com/locate/cattod

X-ray photoelectron spectroscopy (XPS) for catalysts characterization

Anna Maria Venezia*

Istituto per lo Studio dei Materiali Nanostrutturati (ISMN), Sezione di Palermo, Via Ugo La Malfa 153, 90146 Palermo, Italy

Abstract

The general principles of X-ray photoelectron spectroscopy (XPS) as applied in the field of heterogeneous catalysis are reviewed. In particular, the use of this technique in the determination of chemical and physical changes of catalysts upon exposure to gaseous molecules and upon different thermal treatments is examined. Furthermore, examples of methods useful in obtaining the dispersion of supported catalysts are described and, for this purpose, theoretical models of the particle-support distribution are also discussed. The XPS characterization of supported Pd–Ag catalysts is reported, emphasising the advantages of using XPS to investigate surface segregation processes. In the case of supported Pd/Pt bimetallic catalysts it is shown how both, Auger and photoelectron peaks, characterized by different kinetic energies, allow to get depth profile non-destructive analysis. Finally the surface behaviour of CoMo catalysts, used for hydrodesulfurization reactions, is investigated on different supports and under different pre-treatment and reaction conditions.

Keywords: X-ray photoelectron spectroscopy; Supported catalysts; Pd/Ag catalysts; Pd/Pt catalysts; CoMo/silica catalysts

1. Introduction

Heterogeneous catalysis is based on reactions occurring on active sites located at the surface of the catalyst. The reaction proceeds by a sequence of elementary steps including adsorption, surface diffusion, chemical rearrangements of the adsorbed reaction intermediates and desorption of the products [1]. For the development of new catalytic systems it is extremely important to investigate the changes of the surface electronic, chemical and structural properties during a particular process. Analytical techniques, such as X-ray photoelectron spectroscopy (XPS or ESCA) and X-ray excited Auger electron spectroscopy (XAES), based on the detection of ejected electrons, are the most suitable methods for the analysis of surfaces because they probe a limited depth of the sample [2,3]. A limit of these techniques for applications in heterogeneous catalysis is represented by the high vacuum environment required rather than real catalytic working conditions such as atmospheric or even high pressure environments. Nevertheless, the analysis of the surface during exposure to low pressure gases gives important information on the precursor stages of a chemical process [4,5]. In the following, the information obtained by this technique, relevant to the field of catalysis will be outlined.

2. General background

XPS is based on the photoelectric effect arising when high energy photons (usually in the keV range)

* Tel.: +39-91-6809372; fax: +39-91-6809399.
E-mail address: anna@ictpn.pa.cnr.it (A.M. Venezia).

0920-5861/02/$ – see front matter
PII: S0920-5861(02)00380-2

hit a material with the consequent emission of electrons (photoelectrons). The photoelectron kinetic energy, E_k, which is the measured quantity in the experiment, is given by Einstein's law

$$E_k = h\nu - E_b \quad (1)$$

where $h\nu$ is the energy of the incident radiation and E_b the binding energy of the electron in a particular level. If the incident photon is sufficiently energetic, many different levels in the sample may be ionized and thus a spectrum is produced displaying all accessible energy levels as a distribution of photoelectrons with kinetic energies governed by Eq. (1) [6].

Photoelectron peaks are labelled according to the quantum numbers of the level from which the electron originates. The electron is characterized by a total momentum number $j = l + s$, where l is the orbital momentum number and s the spin momentum number which is equal to 1/2 or −1/2. Therefore, whenever $l > 0$, the peak is split into a doublet, with an energy difference called *spin-orbit splitting* which increases with Z roughly as Z^5 [6,7]. The intensity ratio of the two components is determined by the ratio of the multiplicity $(2j + l)$ of the corresponding levels. Additional peaks due to the so called electron *shake-up* process sometimes appear on the high binding energy side of a photoelectron peak. These features correspond to photoelectrons emitted from an atom in which a second electron in a given orbital goes into an excited state as consequence of the sudden change in the atom central potential produced by the photoelectron ejection. The presence of these types of peaks may be quite useful for chemical state determinations.

As a consequence of the primary ionization process, a hole in the core level is created and the excited ion tends to relax by photoemission or by emission of electrons through the Auger decay. The latter is the favourite mechanism for core levels with binding energies below 2 keV. The Auger effect is a multiple ionization process in which an electron from an external level fills the vacancy created in the core level and the difference between the two energy levels is carried away by the ejected Auger electron. The final state is therefore a doubly ionized state with two vacancies in the levels involved in the process. The notation used for the identification of Auger peaks considers all the levels involved in the process. For example, an Auger process referred as KL_2L_3 arises from a ionization of the core electron of the 1s (K) level followed by a contemporary filling of the hole by an electron from the $2p_{1/2}$ (L_2) level and the emission of an electron from the level $2p_{3/2}$ (L_3) or vice versa. The energy of the Auger transition is given by:

$$E_{KL_2L_3} = E_K - E_{L_2} - E_{L_3} - F(L_2L_3; X) + R(L_2L_3) \quad (2)$$

where E indicates the binding energies of the involved levels, $F(L_2L_3; X)$ the Coulombic interaction energy between the two holes in the final state, X, and $R(L_2L_3)$ is a relaxation term referring to the collapse of the passive electron orbitals in the doubly ionized state. As shown in Eq. (2), the kinetic energy of the Auger electrons is related only to the binding energies of the three levels involved in the transition and is independent on the incident energy. Therefore Auger peaks can be distinguished from photoelectron peaks by changing the excitation photon energy which affects only the position of the photoelectron peaks. Both binding energies and Auger energies give information on the chemical environment of the emitting atom.

The XPS technique yields quantitative and qualitative information. Quantitative information arises from the element specificity of the binding energies and the relation between the intensity of the photoelectron peaks and the element concentration. Qualitative information are obtained from the energy position of a photoelectron peak with respect to the energy position of the same level in a reference compound (chemical shift).

2.1. Qualitative information

Chemical shifts of binding energies of a certain element level are due to different oxidation states and different chemical environments. They are interpreted in terms of a simple electrostatic theory, called "charge potential model" [8,9]. According to the model, the energy of the atom is divided into two terms, one associated with the net charge on the probe atom and the other term associated with the charge distribution of the surrounding atoms. Both terms are considered as "initial state effect" since they refer only to the electrostatic potential experienced by the core electron in the ground state before ionization. A more realistic theory takes into account the relaxation effects involved

in the redistribution of the electronic charge during ionization, and referred to as "final state effect". The binding energy chemical shift of a level of the atom i in a molecule with respect to a reference can then be expressed as

$$\Delta E_b = \frac{\Delta q_i}{r_v} - \frac{\sum \Delta q_i}{r_{ij}} - \Delta R \quad (3)$$

The first term on the right represents the electrostatic potential due to the valence charge on atom i with an average valence orbital radius r_v. The summation term is the sum of the potentials at atom i due to the surrounding atoms j considered as point charges. ΔR is the relaxation term.

Like the binding energy chemical shifts, the Auger peak shifts are related to chemical properties. According to the relaxation potential model (RPM) [10,11], the chemical shift, ΔE_b, and the Auger shift, ΔE_k, are equal to:

$$\Delta E_b = \Delta V - \Delta R_{(K)} \quad (4)$$

$$\Delta E_k = -\Delta V + 3\Delta R_{(K)} \quad (5)$$

where ΔV corresponds to the first two terms of Eq. (3), it represents the change in the electrostatic potential felt by the K (1s) core electron of a particular atomic species; $\Delta R_{(K)}$ is the extra-atomic relaxation energy representing the electronic response of the molecular environment of the atom to the creation of the core hole in level K. The combination of Eqs. (4) and (5) gives the "Auger parameter" shift

$$\Delta\alpha = \Delta E_b + \Delta E_k = 2\Delta R_{(K)} \quad (6)$$

Binding energy shifts and Auger energy shifts may be of opposite sign. Variations in Auger parameters are usually larger than Auger and chemical shifts and, since they are not affected by charging and energy reference problems, are often used for electronic charge determination [12].

2.2. Quantitative information

The use of the technique for sample composition analysis is based on the linear relation between the intensity of the signal I_A from element A and its atomic concentration C_A. Thus, for a surface layer

$$I_A = FkS\sigma_A C_A L(\theta) \quad (7)$$

where F is the intensity of the incident photons, k is an instrumental factor and S is the sample analysed area. All three parameters are constant for a given instrumental configuration. The parameter σ_A is the cross-section for the emission of the photoelectron. Cross-sections for the various elements and for the different excitation energies have been tabulated by Scofield [13]. $L(\theta)$ is the angular asymmetry factor, depending on the angle θ between the direction of propagation of the photons and the direction of the outgoing electrons, which describes the intensity distribution of the photoelectrons. When thick materials are probed, the inelastic mean free path (IMFP) of the electrons, indicated with λ, and representing the distance that the electrons can travel inside the solid without suffering inelastic collision, should be considered. Eq. (7) is corrected by an attenuation factor taking into account the angle of the electron detection with respect to the surface (take-off angle ϕ). Then, the XPS peak intensity I_d from a layer of material of thickness d is given by the following equation

$$I_d = I_\infty(1 - e^{-d/\lambda \sin\phi}) \quad (8)$$

where I_∞ is the intensity from an "infinitely' thick layer for electrons of IMFP $= \lambda$ and $\lambda \sin\phi$ is referred to as "effective escape depth". Values of λ versus kinetic energy have been experimentally determined for many solids. It was found a minimum value for energies around 100 eV above which the IMFP varies as the square root of the electron energy [14]. According to Eq. (8), the surface sensitivity of the photoelectron spectroscopy can be enhanced by changing the detection angle ϕ. This feature is exploited to perform depth profile in a non-destructive way. Another non-destructive depth profiling technique is based on the comparison of two photoelectron lines or Auger lines, one at low and the other at high kinetic energies, probing different depths.

Because of its surface enhanced sensitivity, XPS represents a valid tool for particle size determination. Indeed XPS intensity ratios of particle related peaks I_p and support related peaks I_s are strongly dependent on the catalyst dispersion. Qualitatively, catalysts with the same loading of metal over the same support exhibit high I_p/I_s values in the case of small particles as compared to large particles.

The estimate of size from XPS data is not simple and modelling of the supported catalyst is needed.

Several approaches exist which take into account the morphology of the supports in terms of surface area and porosity. Angevine et al. [15] considered a catalyst as formed by crystallites on a semi-infinite support. This assumption was too simple and the predicted values of I_p/I_s were too high especially in the case of a high surface area support. A more realistic model for high area supports was proposed by Kerkhof and Moulijn [16] who considered the catalysts as a series of slabs with cubic particles of sizes c in between. The thickness t of the slabs are estimated from the density ρ and the specific surface area S_0 of the support, according to

$$t = \frac{2}{\rho} S_0 \tag{9}$$

The model assumes that the electrons leave the sample in a direction perpendicular to the surface. The dimensionless sizes β_1, β_2 and α of the support thickness and of the crystallite are defined as

$$\beta_1 = \frac{t}{\lambda_{ss}}, \quad \beta_2 = \frac{t}{\lambda_{ps}}, \quad \alpha = \frac{c}{\lambda_{pp}} \tag{10}$$

where λ being the IMFP for the electrons from the support s or from the metal particle p escaping through the support or through the metal. Then, in the case of supported metal crystallites, the relation between the intensity ratio of metal over support photoelectron peaks (I_p/I_s) and the bulk atomic concentration $(p/s)_b$ is the following:

$$\left(\frac{I_p}{I_s}\right) = \left(\frac{p}{s}\right)_b \left(\frac{\sigma_p}{\sigma_s}\right) \left(\frac{\beta_1}{2}\right) \left[\frac{1 + e^{-\beta_1}}{1 - e^{-\beta_2}}\right] \left[\frac{1 - e^{-\alpha}}{\alpha}\right] \tag{11}$$

where σ_p and σ_s are the photoelectron cross-sections of the considered photoelectron peaks. In the case of a monolayer distribution of the supported metal, the dimensionless size α is so small that the last factor of Eq. (11) is equal to 1 and the following expression is obtained

$$\left(\frac{I_p}{I_s}\right) = \left(\frac{p}{s}\right)_b \left(\frac{\sigma_p}{\sigma_s}\right) \left(\frac{\beta_1}{2}\right) \left[\frac{1 + e^{-\beta_1}}{1 - e^{-\beta_2}}\right] \tag{12}$$

by substituting all the known parameters in Eq. (12) the intensity ratio of the monolayer catalysts can be calculated. The relation between the experimental I_p/I_s which, according to the model is given in Eq. (11) and the monolayer intensity ratio calculated according to Eq. (12) is the following

$$\frac{(I_p/I_s)_{\text{crystallite}}}{(I_p/I_s)_{\text{monolayer}}} = \frac{1 - e^{-\alpha}}{\alpha} \tag{13}$$

By plotting this relation for different value of α, an estimate of the crystallite sizes is obtained. Reliable values of the sizes are dependent on cross-section values, on electron IMFPs and on support surface areas. Calculated Scofield [13] cross-sections and IMFPs obtained according to an empirical formula by Seah and Dench [14] have given satisfactory results.

3. Experimental apparatus

The main components of a XPS instrument are the X-ray source, the electron energy analyser, the electron detector and an efficient pumping system for the high vacuum requirement. The laboratory conventional source consists of a X-ray tube where X-rays are generated by electron bombardment of magnesium or aluminium from which the $K\alpha_{1,2}$ radiation is produced. Moreover synchrotron radiation can be used to provide a continuous source of photons in the range 0.1–10 keV. The analysis of the electron energy spectrum is performed by an electron velocity analyser, called spectrometer, of the electrostatic type. The concentric hemispherical analyser (CHA) is one of the most used in commercial spectrometers. An important parameter of the analyser is its energy resolution which can be referred to as absolute or relative. The absolute resolution (ΔE) is defined as the full width at half maximum height (FWHM) of a given peak. The relative energy resolution is defined as the ratio $R = \Delta E/E_0$ between ΔE and the kinetic energy E_0 of the peak position. The FWHM depends on the X-ray source line width, the analyser broadening and the intrinsic line width of the considered level. It is common practice to retard the electrons at the entrance of the analyser to a constant energy called “pass energy”, in order to have the smallest absolute resolution. Analysers generally operate in the constant (or fixed) analyser energy (CAE) mode where the absolute energy resolution does not depend on the analyser contribution and is constant for a determined value of pass energy.

Since the kinetic energy of the outgoing electron is affected by the charge accumulated on the sample during the ejection of photoelectrons, calibration with respect to the energy of a reference peak is needed. When dealing with supported catalysts, electrons from the support can be used as internal reference. If not available, the C 1s binding energy, set at 284.4–285.0 eV, arising from carbon contamination can be used.

Careful data analysis can assist in obtaining the maximum amount of information. The peaks are generally fitted by a non-linear least square fitting routine using a weighted sum of Lorentzian and Gaussian component curves after removal of background. Details on data processing can be found in Ref. [7].

4. Application of XPS to catalysis

4.1. XPS study of pumice supported palladium catalysts

The XPS technique has been applied for the characterization of several pumice supported catalysts used in the hydrogenation of 1,3-cyclooctadiene to cyclooctene [12,17]. The catalytic activities of palladium catalysts with different metal loading and different metal particle sizes, as obtained from X-ray diffraction (XRD) measurements, have been analysed [17]. The Pd $3d_{5/2}$ chemical shifts (ΔE $3d_{5/2}$), the Auger parameter shifts ($\Delta\alpha$) obtained from Pd $3d_{5/2}$ and Pd_{MNN} Auger shifts (Eq. (6)), the relaxation energy shifts (ΔR_{ea}), the potential shifts (ΔV) and electronic charge variations (Δq) for Pd/pumice catalysts with respect to the palladium powder reference are given in Table 1 [12]. The relaxation energy shifts and the potential shifts were calculated using Eqs. (4)–(6). The charge term (Δq) was calculated according to Eq. (3). The first term represents the chemical effect due to change in the charge distribution of the valence shell of the photoemitting atom and the second term is the variation of the inter-atomic potential and represents the matrix effect. For large metal particles, with electronic properties similar to palladium powder, the first term of the Eq. (3) was neglected. Therefore from the potential shift of the catalyst labelled as W7 it was possible to obtain the potential term relative to the support effect which was assumed to be the same for all catalysts. The excess of negative charge on the small palladium clusters was calculated. In Figs. 1 and 2 the Auger parameter and the catalytic activity, expressed as turnover frequency (TOF), versus particle size are reported. The two sets of data show a dependence of the catalytic activity on the electronic charges.

4.2. Determination of supported particle sizes

One of the most important properties of supported metal catalysts, which allows to compare the catalytic activities, is the dispersion of the active species determined by particle sizes. Chemisorption and X-ray diffraction methods are commonly used in the determination of the particle dimensions. Both methods, however, have their limitation since the former depends on the adsorption capability of the particular metal and requires an accurate knowledge of the adsorption stoichiometry, the latter does not allow to detect particles of sizes below 2–5 nm. The application of Kerkhof and Moulijn's [16] method to Pt/SiO_2 catalysts allowed to determine catalyst dispersion in

Table 1
Palladium (wt.%), XRD metal particle diameters d (Å), Pd $3d_{5/2}$ chemical shifts (ΔE $3d_{5/2}$), Auger parameter shifts ($\Delta\alpha$), relaxation energy shifts (ΔR_{ea}), potential shifts (ΔV), and electronic charge variations (Δq) for Pd/pumice catalysts with respect to palladium metal powder

Samples	Pd (wt.%)	d (Å)	ΔE $3d_{5/2}$ (eV)	$\Delta\alpha$ (eV)	ΔR_{ea} (eV)	ΔV (eV)	Δq (a.u.)
W0	0.05	1	−1.0	−2.0	−1.0	−2.0	−0.148
W1	0.20	22	−0.6	−1.2	−0.6	−1.2	−0.072
W2	0.11	29	−0.3	−0.9	−0.45	−1.15	−0.07
W3	0.39	35	−0.4	−0.5	−0.25	−0.65	−0.02
W4	0.61	35	−0.6	−0.2	−0.1	−0.7	−0.02
W5	0.86	40	−0.4	−0.2	−0.1	−0.5	−0.005
W6	0.30	50	−0.5	−0.2	−0.1	−0.6	−0.015
W7	1.05	81	−0.4	−0.1	−0.05	−0.45	0

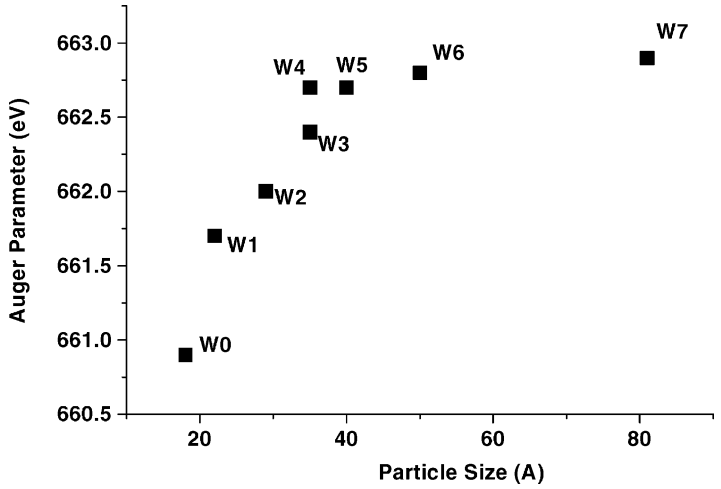

Fig. 1. Palladium Auger parameter of the catalysts versus palladium particle sizes.

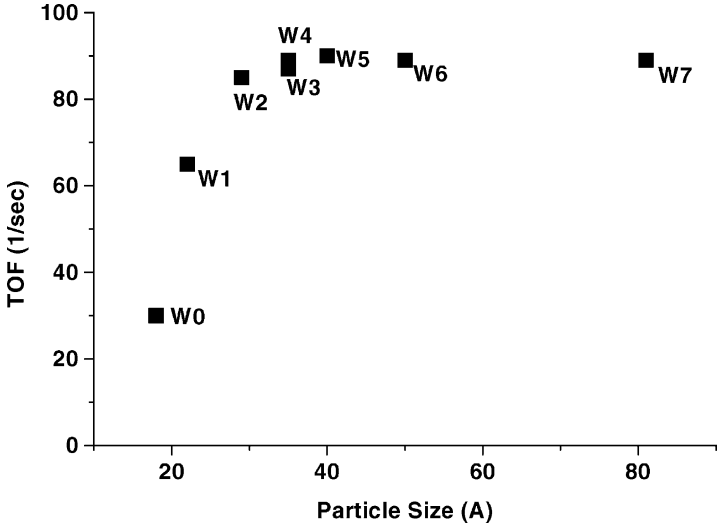

Fig. 2. TOF of the selective hydrogen reduction of the 1,3-cyclooctadiene to monoene versus palladium particle sizes of the catalysts.

agreement with chemisorption measurements. The reliability of this model and other related ones lies on the assumption of a sample homogeneity and crystallite size uniformity.

A different approach, using the experimental intensity ratio for two core levels with different kinetic energies arising from the same dispersed phase has been developed by Davis [18]. The advantage of this approach is a certain independence from the physical properties of the catalysts such as surface area and supported phase loading and distribution. According to the model, the final expression for the particle size of cubic crystallites is obtained by iteration of the following equation

$$d = -\lambda_1 \ln\left[1 - \left(\frac{\sigma_2 T_2 \lambda_2 I_2}{\sigma_1 T_1 \lambda_1 I_1}\right)\left(1 - \exp\left(\frac{-d}{\lambda_2}\right)\right)\right] \quad (14)$$

where T represents the instrumental detection efficiency, depending on the kinetic energy of the photoelectron, and the other parameters are as defined above, with index 1 and 2 referring to two different core level processes. In the case of a 3.3 wt.% Pd/Al_2O_3 sample, prepared by impregnation, the sintering behaviour after calcination treatments at various temperature was followed by collecting the Pd 3d and Pd_{MNN} Auger spectra [18]. The particle sizes obtained from the XPS data were in good agreement with electron microscopy results. Discrepancies arose in the case of large particles due to the loss of sensitivity of the XPS intensity ratio for particle sizes above 3λ.

Within the approaches mentioned above, a limit to the accuracy of particle size estimation from photoemission data is represented by the presence of contaminant over-layers, which would attenuate the peak with lower kinetic energy. For this reason, particular care should be taken to obtain clean surfaces.

4.3. Determination of surface segregation processes on bimetallic catalysts

In particular reactions, supported bimetallic systems show superior catalytic performance in terms of activity and selectivity with respect to monometallic catalyst [20,21]. In most cases the surface composition of the particles is different from the bulk composition. Therefore bulk methods like X-ray diffraction do not provide helpful information. Chemisorption measurements can help to discriminate the metal sites at the surface, however its use is limited to the chemisorption capability of the particular metals and cannot be of general use. With XPS analyses, by exploiting changes in the sampling depths of photoelectrons ejected from different core levels of the same element, it is possible to detect concentration gradients in metal aggregates. As examples of application of this method the study of two series of bimetallic catalysts, pumice supported Pd/Pt and pumice supported Pd/Ag catalysts, will be illustrated [19,22].

Concerning the first series of samples, the intensity ratios, $I(Pd\ 3d_{3/2})/I(Pd_{MNN})$, along with the XPS derived atomic ratios, the bulk atomic ratios and the particle sizes, for a series of pumice supported Pd/Pt catalysts are reported in Table 2 [19]. The corresponding intensity ratio for palladium foil is reported since it represents the reference value for a homogeneous palladium distribution. Comparison of the atomic ratios of Pd/Pt, obtained from the quantitative analysis of the areas of the Pd $3d_{3/2}$ and Pt 4f peaks, with the bulk atomic ratios allowed to determine the preferential surface segregation of the metals. The component Pd $3d_{5/2}$ was not considered because it overlapped with the tail of the Pt $4d_{3/2}$ peak. According to the results, the palladium enriched samples were surface depleted in palladium, whereas the platinum rich ones had similar surface and bulk composition. The intensity ratio of the two palladium peaks, the Pd $3d_{3/2}$ with kinetic energy of ∼1150 eV (with the aluminium anode), probing deeper layers, and the Auger Pd_{MNN} with kinetic energy ∼325 eV, probing shallower layers were normalized with respect to the size of the particles. Therefore, they were divided by the term $[1-\exp(-d/\lambda^{3d})]/[1-\exp(-d/\lambda^{MNN})]$, where d is the size of the metal particles, as obtained by X-ray diffraction of the metal particles and λ^{3d} and λ^{MNN} are the mean free paths of the two different ejected electrons. From the intensity ratios of the two palladium lines listed in Table 2 among the platinum rich samples it was possible to ascertain surface segregation of palladium. The observed difference between the corresponding ratios for Pd metal foil and for the monometallic Pd_{100} was attributed to matrix effects. In the same study negative chemical shifts of 0.5 eV of Pd 3d and Pt 4f with respect to standards of both metals were attributed to the metal-support interaction through the basic OH sites of the support [19]. The XPS characterization of the pumice supported catalysts allowed to correlate the decreased hydrogenation

Table 2
XPS derived and bulk atomic ratios along with metal particle sizes determined by X-ray diffraction spectroscopy and normalized intensity ratio $I(Pd\ 3d_{3/2})/I(Pd_{MNN})$ for pumice supported Pd/Pt catalysts [19]

Samples	$(Pd/Pt)_{XPS}$	$(Pd/Pt)_{bulk}$	d (Å)	$I(Pd\ 3d_{3/2})/I(Pd_{MNN})$
Pd foil				0.26
Pd_{100}			18	0.45
$Pd_{99/1}$	n.d.	n.d.	42	0.44
$Pd/Pt_{95/5}$	13.2	31.7	27	0.41
$Pd/Pt_{90/10}$	7.0	17.3	24	0.43
$Pd/Pt_{3/1}$	4.0	4.2	28	0.37
$Pd/Pt_{2/2}$	1.6	1.8	35	0.35
$Pd/Pt_{1/3}$	1.0	0.8	50	0.31
$Pd/Pt_{10/90}$	0.3	0.2	52	0.21

Table 3
Ag $3d_{5/2}$ and Pd $3d_{5/2}$ binding energies (eV) and XPS derived atomic ratios, Ag/Si, Pd/Si and Ag/Pd, of the various pumice supported catalysts after different treatments

Catalyst	Ag $3d_{5/2}$	Pd $3d_{5/2}$	Ag/Si	Pd/Si	Ag/Pd
0.6Ag as prepared	368.2		3.3		
Oxidized	368.2		0.0		
Reduced	367.7		5.9		
0.27Pd as prepared		334.5		1.6	
Oxidized		336.6		1.2	
Reduced		335.1		2.7	
0.27Pd0.13Ag as prepared	367.0	334.7	0.8	1.1	0.7
Oxidized	–	337.2	0.0	0.5	0
Reduced	367.0	334.4	2.3	0.9	2.5
0.3Pd0.6Ag as prepared	368.2	335.2	2.2	0.8	2.7
Oxidized	368.3	337.0	0.6	0.6	1
Reduced	367.5	334.8	3.5	0.6	5.7
0.6Ag0.3Pd as prepared	368.2	336.0	1.8	0.8	2.3
Oxidized	368.4	336.7	1.4	1	1.4
Reduced	367.6	334.8	4.4	1	4.4
0.6Ag0.5Pd as prepared	368.0	335.0	2.8	0.8	3.3
Oxidized	368.0	336.6	0.6	0.8	0.8
Reduced	367.5	334.8	3.2	0.7	4.4

activity of the bimetallic catalysts with respect to monometallic Pd catalyst with both electronic and structural effects [21].

A series of supported Pd/Ag catalysts, with different metal loadings prepared from organometallic precursors, has been tested in the catalytic oxidation of CO at 523 K [22]. The samples were used "as received", after oxidation and after reduction at 623 K. A detailed XPS analysis of the samples before each catalytic test was performed. In Table 3 the binding energies along with the XPS derived atomic ratios are listed. The Ag 3d and Pd 3d binding energies in the "as received" and reduced samples are indicative of metallic states for both elements. The Ag $3d_{5/2}$ negative shift found in the "as received" 0.27Pd0.13Ag/pumice could be explained by electronic effect arising from the closeness to palladium atoms [23]. The Pd 3d binding energies obtained after the oxidation treatments are indicative of the formation of PdO [24]. On the contrary, as indicated from the Ag 3d binding energies, the oxidation state of metallic silver is not changed. It is known that silver oxides are quite unstable and the two silver oxides, Ag_2O and AgO, decompose at 503 and 373 K, respectively, even in oxygen atmosphere [25]. It is worth mentioning the decrease of Ag $3d_{5/2}$ binding energy after reduction treatment with respect to the "as received" sample. The possible explanation can be a larger interaction with the pumice support due to an increased dispersion of the metal particles caused by the high temperature air treatment followed by H_2. This statement is supported by the increased Ag/Pd atomic ratio derived from XPS measurements.

The photoelectron spectra of the bimetallic 0.3Pd0.6Ag/pumice catalyst, after in situ gas treatments, are shown in Fig. 3. From the relative intensity ratio of the Ag 3d and the support K 2s photoelectron peaks occurring in the same energy region, it appears that silver, in air environment at 623 K, diffuses away from the surface and reappears after treatment with H_2 at the same temperature. According to the XPS derived Ag/Pd atomic ratios, all the analysed samples exhibited silver enriched surface in the "as received" and reduced states and silver depleted surface in the oxidized state. The surface enrichment of silver in bulk Pd–Ag systems is well known and is attributed to the lower surface energy of silver with respect to palladium [26].

The CO oxidation activity decreased with the increased amount of silver in the bimetallic catalysts as compared to the monometallic Pd catalyst. Addition of silver was detrimental for any pre-treatment

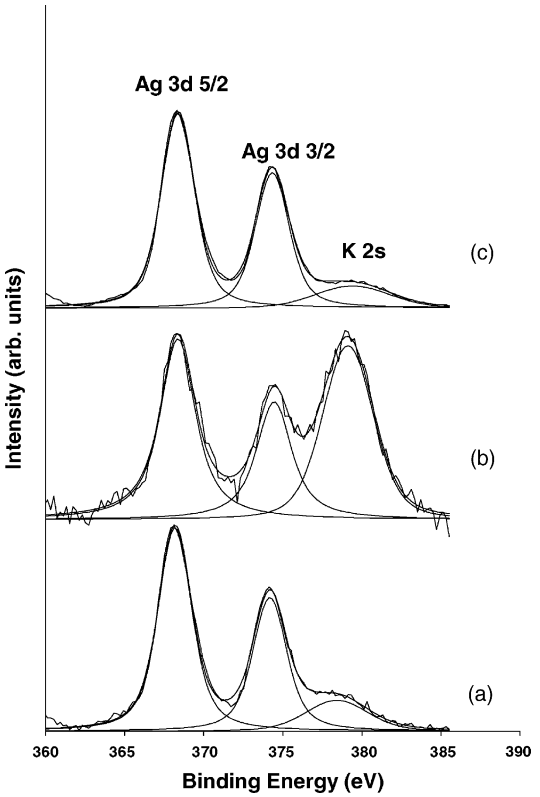

Fig. 3. Ag 3d XPS spectra of 0.3Pd0.6Ag/pumice catalyst in the: (a) as received; (b) oxidized; (c) reduced state.

conditions. For each sample, the CO conversion increased after air treatment at 623 K. In this case, the catalyst surface consisted mainly of partially oxidized palladium and some metallic silver particles. After reduction at 623 K, the catalysts were always more active even if the silver to palladium surface ratio increased as shown in Table 3. According to the XPS analyses, the catalyst treatments determined the following structures: (i) the "as received" samples were formed mainly by particles of palladium partially covered by silver which diminished the activity with respect to the Pd monometallic sample; (ii) the oxidation treatment drove the silver into the bulk, in accord with the decreased $(Ag/Pd)_{XPS}$ ratio, exposing the palladium surface which was in a partially oxidized state and exhibited higher activity; (iii) the reduction treatment produced active palladium metal particles in proximity of inert silver particles which, as indicated by the increased $(Ag/Pd)_{XPS}$ ratio and the unchanged $(Pd/Si)_{XPS}$ ratio were dispersed on the support rather than covering the palladium particles. The presence of silver particles could contribute to the increased conversion of CO by oxygen activation [25].

4.4. Characterization of Mo based HDS catalysts

CoMo catalysts supported on silica with and without sodium, prepared with different procedures, such as the sol–gel route, the classic wet impregnation and the co-impregnation of commercial silica or sol–gel prepared silica were tested in the hydrodesulfurization of thiophene [27]. According to the X-ray diffraction analyses most of the samples were amorphous except those calcined at temperatures higher than 773 K exhibiting crystalline β-$CoMoO_4$ sodium molybdates. No correlation between the structure and the activity could be found. The XPS technique, through the detection of the Co 2p, Mo 3d and Si 2p photoelectrons allowed to determine the oxidation states of the precursor oxides and of the spent catalyst after HDS reactions. Moreover the effect of sodium on the molybdenum electron properties was evidenced. As indicated from the spectra of Fig. 4, a better resolution of the Mo 3d doublet with the consequent narrowing of each component was found for the sodium containing samples. Such effect, independent from the preparation procedure, depended on the amount of sodium. According to a recent study [28] and to previous work on CoMo catalysts supported on alumina [29], the presence of sodium in the support, favours the adsorption of Mo via the monomeric species MoO_4^{2-} rather than polymeric species by increasing the local pH. Moreover sodium might inhibit the formation of Mo(V) caused by reducing the action of NH_3 formed by decomposition of the ammonium salt deposited in the pores [30]. The combination of these two effects would result in narrower Mo 3d spectra for the sodium containing catalysts.

A typical Mo 3d spectrum, after HDS reaction is shown in Fig. 5 for the sol–gel prepared catalyst, $CoMo/SiO_2$. The spectral region contains a S 2s peak and three Mo 3d doublets. The unreduced Mo(VI) component is found at ∼232 eV. The doublet with the main Mo $3d_{5/2}$ peak at ∼228.4 eV is typical of Mo(IV), in oxidic or sulfidic forms [31,32]. The additional doublet characterized by Mo $3d_{5/2}$ at 229.6 eV is attributed to the intermediate reduced state Mo(V).

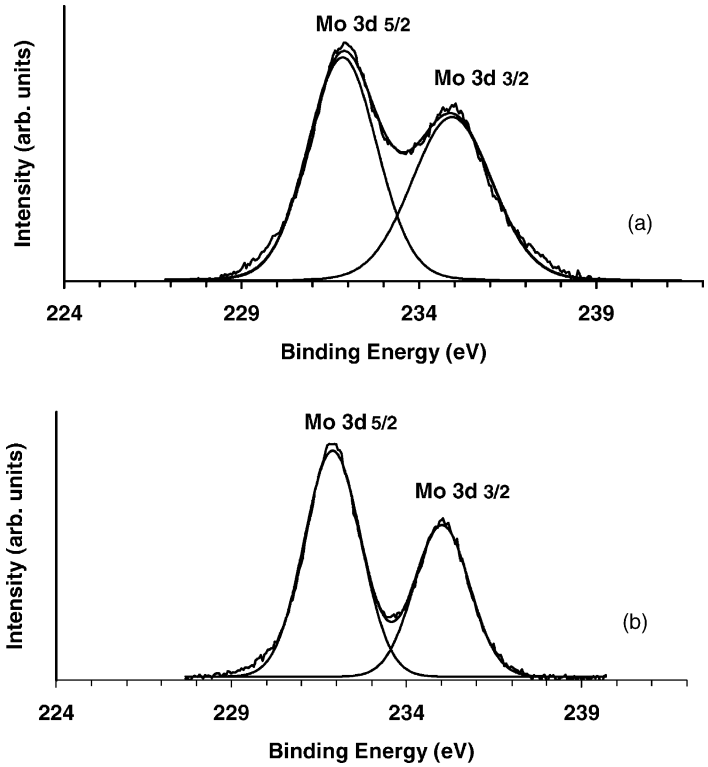

Fig. 4. Mo 3d spectra of the $CoMo/SiO_2$ prepared by sol–gel: (a) without sodium; (b) with 2.8 wt.% Na.

Typical XPS spectra of Co 2p before and after the HDS reaction are shown for the sol–gel prepared catalyst $CoMo/SiO_2$ in Fig. 6a and b, respectively. The spectra contains the spin-orbit components Co $2p_{3/2}$ at 780.3 eV and the Co $2p_{1/2}$ at 796.2 eV. On the basis of the binding energies, spin-orbit coupling and satellites (shake-up), the peaks are attributed to Co^{2+} present as CoO or $CoMoO_4$ [33]. Upon HDS reaction,

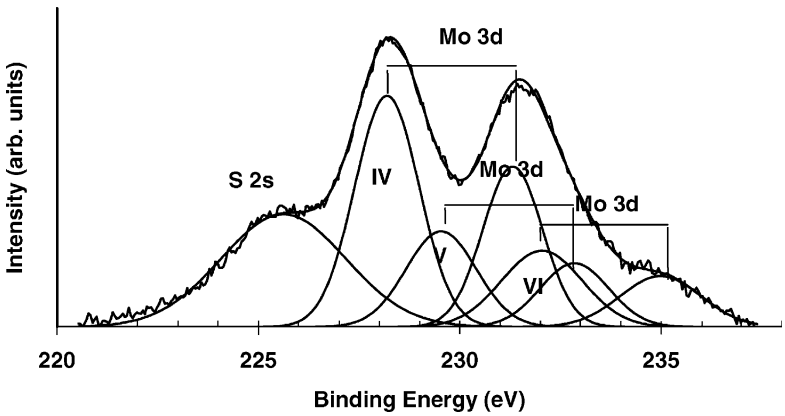

Fig. 5. S 2s and Mo 3d spectra of $CoMo/SiO_2$ prepared by sol–gel after HDS reaction.

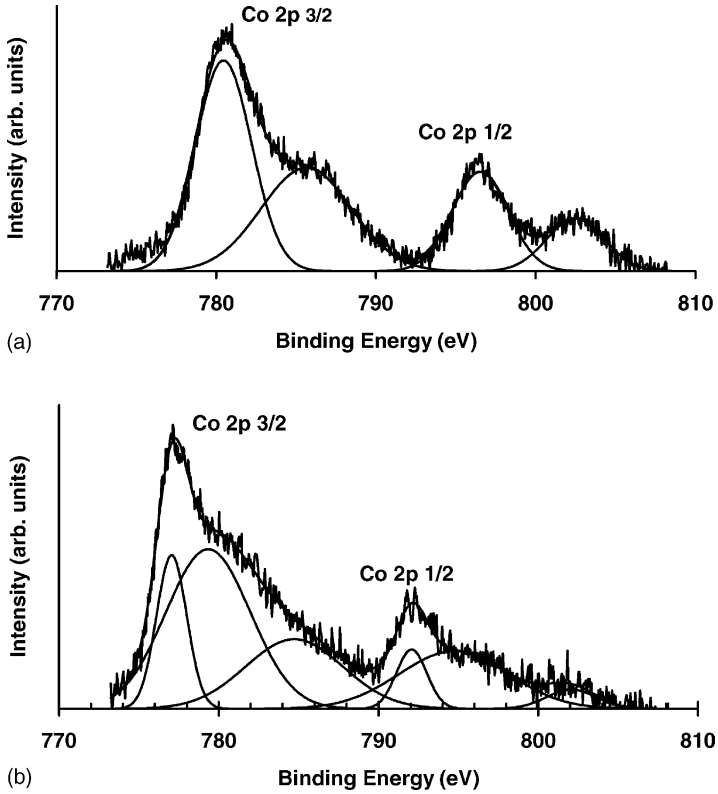

Fig. 6. Co 2p spectra of $CoMo/SiO_2$ prepared by sol–gel: (a) calcined at 823 K; (b) after HDS reaction.

Co 2p spectra modified as shown in Fig. 6b. Sharper Co 2p components, found at lower binding energies (777–778 eV) are attributed to sulfided cobalt species or to reduced cobalt Co^0, practically indistinguishable [34]. The comparison of Co 2p/Mo 3d intensity ratio of the samples before and after reaction, indicates that cobalt has tendency to segregate to the surface during HDS reaction. The presence of sulfur after reaction is confirmed by the peaks of S 2p at 161.5 eV and S 2s at 225.6 eV (Fig. 5). Upon HDS reaction, surface enhancement of sodium occurs on alkali ion doped catalysts. Moreover, a 50% decrease of the intensity of the carbon peaks is observed in the sodium doped samples as compared to the undoped catalysts. Such decrease indicates a beneficial effect of sodium in reducing the "coke" formation, one of the main cause of catalyst poisoning. A relation between the catalytic activity and the surface S/Mo(IV) atomic ratio after the HDS was found. Accordingly, the most active catalyst had the largest ratio to which MoS_2 and some mixed Mo(V) oxysulfide contributed. The least active catalyst contained hard to reduce MoO_2.

5. Conclusive remarks

The XPS technique allows an analytical and chemical characterization of solid materials. Due to the limited escape depth of the photoelectrons, and in consideration of the fact that the part of catalysts most involved in the catalytic reactions is limited to the topmost layers, the technique is particularly suitable for the understanding of the electronic and morphological structure of heterogeneous catalysts. Moreover XPS is an important tool for studying the dispersion of supported catalysts, especially when other techniques such as X-ray diffraction or chemisorption fail to give meaningful results. However, development of good theoretical models for particular catalyst systems are needed in order to extract

from the XPS measurements information on particle sizes.

References

[1] G.A. Somorjai, Introduction to Surface Chemistry and Catalysis, Wiley, New York, 1994.
[2] C.J. Powell, D.M. Hercules, A.W. Czanderna, in: A.W. Czanderna, D.M. Hercules (Eds.), Ion Spectroscopy for Surface Analysis, Plenum Press, New York, 1991, p. 417.
[3] J.W. Niemantsverdriet, Spectroscopy in Catalysis, VCH, Weinheim, 1993.
[4] A.M. Venezia, C.M. Loxton, J.A. Horton, Surf. Sci. 225 (1990) 195.
[5] A.M. Venezia, C.M. Loxton, Surf. Sci. 194 (1988) 136.
[6] T.A. Carlson, Photoelectron and Auger Spectroscopy, Plenum Press, New York, 1975.
[7] D. Briggs, M. Seah, Practical Surface Analysis, Auger and X-ray Photoelectron Spectroscopy, vol. 1, Wiley, New York, 1990.
[8] K. Siegbahn, et al., ESCA Applied to Free Molecules, North-Holland, Amsterdam, 1969.
[9] D.W. Davis, D.A. Shirley, J. Electron Spectr. Relat. Phenom. 3 (1974) 137.
[10] C.D. Wagner, A. Joshi, J. Electron Spectr. Relat. Phenom. 47 (1988) 283.
[11] S.P. Kowalczyk, R.A. Pollak, F.R. McFeely, L. Ley, D.A. Shirley, Phys. Rev. B 8 (1973) 2387.
[12] A.M. Venezia, A. Rossi, D. Duca, A. Martorana, G. Deganello, Appl. Catal. A 125 (1995) 113.
[13] J.H. Scofield, J. Electron. Spectr. Relat. Phenom. 8 (1976) 129.
[14] M.P. Seah, W.A. Dench, Surf. Interf. Anal. 1 (1979) 2.
[15] P.J. Angevine, J.C. Vartulli, W.N. Delgass, in: Proceedings of the Sixth International Congress on Catalysis, vol. 1976, 1977, p. 2.
[16] F.P.J.M. Kerkhof, J.A. Moulijn, J. Phys. Chem. 83 (1979) 1012.
[17] G. Deganello, D. Duca, A. Martorana, G. Fagherazzi, A. Benedetti, J. Catal. 150 (1994) 127.
[18] S.M. Davis, J. Catal. 117 (1989) 432.
[19] A.M. Venezia, D. Duca, M.A. Floriano, G. Deganello, A. Rossi, Surf. Interf. Anal. 19 (1992) 543.
[20] A. Sarkany, Z. Zsoldos, Z. Stefler, Gy. Hightower, L. Guczi, J. Catal. 157 (1995) 179.
[21] G. Deganello, D. Duca, L.F. Lotta, A. Martorana, A.M. Venezia, A. Benedetti, G. Fagherazzi, J. Catal. 151 (1995) 125.
[22] A.M. Venezia, L.F. Liotta, G. Deganello, Z. Schay, D. Horvath, L. Guczi, Appl. Catal. A 211 (2001) 167.
[23] P. Steiner, S. Hufner, Solid State Commun. 73 (1981) 79.
[24] A.M. Venezia, L.F. Liotta, G. Deganello, Z. Schay, L. Guczi, J. Catal. 182 (1999) 449.
[25] A. Nagy, G. Mestl, Appl. Catal. A 188 (1999) 337.
[26] V. Ponec, G.C. Bond, Catalysis by Metals and Alloys, Stud. Surf. Sci. Catal., vol. 95, Elsevier, Amsterdam, 1995.
[27] A.M. Venezia, V. La Parola, G. Deganello, D. Cauzzi, G. Leopardi, G. Predieri, Appl. Catal. A. 229 (2002) 261.
[28] V. La Parola, G. Deganello, C.R. Tewell, A.M. Venezia, Appl. Catal. A 235 (2002) 171.
[29] A. Licourghiotis, C. Defossè, F. Delannay, B. Delmon, JCS Faraday I 76 (1980) 2052.
[30] C. Thomazeau, V. Martin, P. Afanasiev, Appl. Catal. A 199 (2000) 61.
[31] H. Shimada, T. Sato, Y. Yoshimura, J. Hiraishi, A. Nishijma, J. Catal. 110 (1988) 275.
[32] T.I. Koranyi, I. Manninger, Z. Paal, O. Marks, J.R. Gunter, J. Catal. 116 (1989) 422.
[33] Y. Okamoto, T. Imanaka, S. Teranishi, J. Catal. 65 (1980) 448.
[34] T.I. Koranyi, I. Manninger, Z. Paal, Solid State Ion 32 (1989) 1012.